MULTIPATH TIME SPREADING OF OPTICAL PULSES PROPAGATING THROUGH A SCATTERING MEDIUM

AIR FORCE INSTITUTE OF TECHNOLOGY

1975

MULTIPATH TIME SPREADING OF OPTICAL PULSES PROPAGATING THROUGH A SCATTERING MEDIUM

BY

RONALD NOWELL CLEVELAND

B.S., University of Illinois, 1974

THESIS

Submitted in partial fulfillment of the requirements
for the degree of Master of Science in Electrical Engineering
in the Graduate College of the
University of Illinois at Urbana-Champaign, 1975

Urbana, Illinois

UNCLASSIFIED

SECURITY CLASSIFICATION OF THIS PAGE (When Data Entered)

REPORT DOCUMENTATION PAGE		READ INSTRUCTIONS BEFORE COMPLETING FORM
1. REPORT NUMBER CI-76-8	2. GOVT ACCESSION NO.	3. RECIPIENT'S CATALOG NUMBER
4. TITLE (and Subtitle) MULTIPATH TIME SPREADING OF OPTICAL PULSES PROPAGATING THROUGH A SCATTERING MEDIUM		5. TYPE OF REPORT & PERIOD COVERED Master of Science Thesis 6. PERFORMING ORG. REPORT NUMBER
7. AUTHOR(s) RONALD NOWELL CLEVELAND MAJOR, USAF		8. CONTRACT OR GRANT NUMBER(s)
9. PERFORMING ORGANIZATION NAME AND ADDRESS AFIT student at the University of Illinois, Urbana, Illinois		10. PROGRAM ELEMENT, PROJECT, TASK AREA & WORK UNIT NUMBERS
11. CONTROLLING OFFICE NAME AND ADDRESS Air Force Institute of Technology (CI) Wright-Patterson AFB OH 45433		12. REPORT DATE 1974 13. NUMBER OF PAGES 49 pages
14. MONITORING AGENCY NAME & ADDRESS (if different from Controlling Office)		15. SECURITY CLASS. (of this report) Unclassified 15a. DECLASSIFICATION/DOWNGRADING SCHEDULE

16. DISTRIBUTION STATEMENT (of this Report)

Approved for Public Release, Distribution Unlimited.

17. DISTRIBUTION STATEMENT (of the abstract entered in Block 20, if different from Report)

18. SUPPLEMENTARY NOTES

JERRY C. HIX, Captain, USAF
Director of Information, AFIT

APPROVED FOR PUBLIC RELEASE AFR 190-17.

19. KEY WORDS (Continue on reverse side if necessary and identify by block number)

20. ABSTRACT (Continue on reverse side if necessary and identify by block number)

DD FORM 1 JAN 73 1473 EDITION OF 1 NOV 65 IS OBSOLETE

UNCLASSIFIED

SECURITY CLASSIFICATION OF THIS PAGE (When Data Entered)

ACKNOWLEDGEMENT

I would like to thank my advisor, Dr. Henry Merkelo, for furnishing the central concepts upon which this thesis is based, and for providing many useful suggestions for the text. Thanks, also, to the National Science Foundation for their financial support of this work. I am indebted to the United States Air Force for allowing me to pursue advanced studies under the sponsorship of the Air Force Institute of Technology. A special thanks to my wife, Marjorie, for her love, understanding and encouragement which have sustained me throughout the last three years.

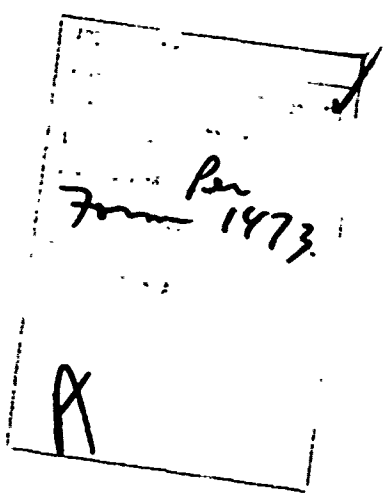

TABLE OF CONTENTS

INTRODUCTION

Historically the problem of propagation of optical energy through a scattering medium first became evident in astronomy. More recently interest in optical communication systems employing atmospheric propagation channels has added additional impetus to the search for analytic models which can predict system performance.

From the communications system viewpoint one may ask: How does a cloud located along the propagation path affect the communication channel? A familiar observation is that significant amounts of sunlight can be observed even through very thick clouds. It seems reasonable to expect that significant amounts of optical signal could be collected provided the receiver's field-of-view (FOV) is increased to collect much of the scattered energy in addition to the unscattered component. Such a scheme introduces multiple paths by which transmitted photons may arrive at the receiver. Thus, multipath time spreading of the optical pulse is a consequence which must be accepted when receiver FOV accomodation is used.

Given the high data rates expected of a viable optical communication system coupled with the fact that the information is transmitted by very short (picosecond) pulses, multipath time spreading of the received pulses can produce intersymbol interference increasing the error rate. Thus, the presence of a scattering medium in the propagation path may force a reduction of the data rate to achieve an acceptable error rate.

Although numerous theoretical treatments of this problem can be found in the literature [1,2,3] very few experimental results have been published. The full scale experiments which have been reported typically specify the scatterer's parameters such as particle size distribution, concentration,

size and shape with little precision. Thus, one objective of this investigation was to conduct a controlled scattering experiment wherein these parameters were known quite precisely. The uniform latex particles in aqueous suspension which were used to simulate water droplets in the atmosphere satisfied this requirement well.

A mode locked He:Ne laser provided optical pulses typical of those encountered in optical communications systems. The time delays generated in this experiment were on the order of tens of picoseconds; this required an indirect measurement scheme which compared the relative phase of the incident and scattered pulse envelopes.

SECTION 1

THEORY

A. Mie Solution

Consider a single dielectric sphere whose center is coincident with the origin of a spherical coordinate system (Fig. 1-1). Suppose a uniform plane wave propagating in the +z-direction is incident upon the sphere of radius a. The scattered fields are given by the solution usualiy attributed to Mie [4]. This solution is exact but of series form.

The values for the far fields ($r >> \lambda$) are given by:

$$E_\theta^s = \frac{-j}{kr} \exp[-jkr]\cos\phi\, S_2(\theta) \tag{1.1}$$

$$E_\phi^s = \frac{j}{kr} \exp[-jkr]\sin\phi\, S_1(\theta) \tag{1.2}$$

where the usual $\exp(j\omega t)$ is assumed for the time dependence and

$$S_1(\theta) = \sum_{n=1}^{\infty} \frac{2n+1}{n(n+1)} \{a_n \pi_n(\cos\theta) + b_n \tau_n(\cos\theta)\} \tag{1.3}$$

$$S_2(\theta) = \sum_{n=1}^{\infty} \frac{2n+1}{n(n+1)} \{b_n \pi_n(\cos\theta) + a_n \tau_n(\cos\theta)\} \tag{1.4}$$

$$a_n = \frac{\psi_n'(\gamma)\,\psi_n(\beta) - m\,\psi_n(\gamma)\,\psi_n'(\beta)}{\psi_n'(\gamma)\,\xi_n(\beta) - m\,\psi_n(\gamma)\,\xi_n'(\beta)} \tag{1.5}$$

$$b_n = \frac{m\psi_n'(\gamma)\,\psi_n(\beta) - \psi_n(\gamma)\,\psi_n'(\beta)}{m\psi_n'(\gamma)\,\xi_n(\beta) - \psi_n(\gamma)\,\xi_n'(\beta)} \tag{1.6}$$

$$\psi_n'(z) = \frac{d}{dz}\psi_n(z) \tag{1.7}$$

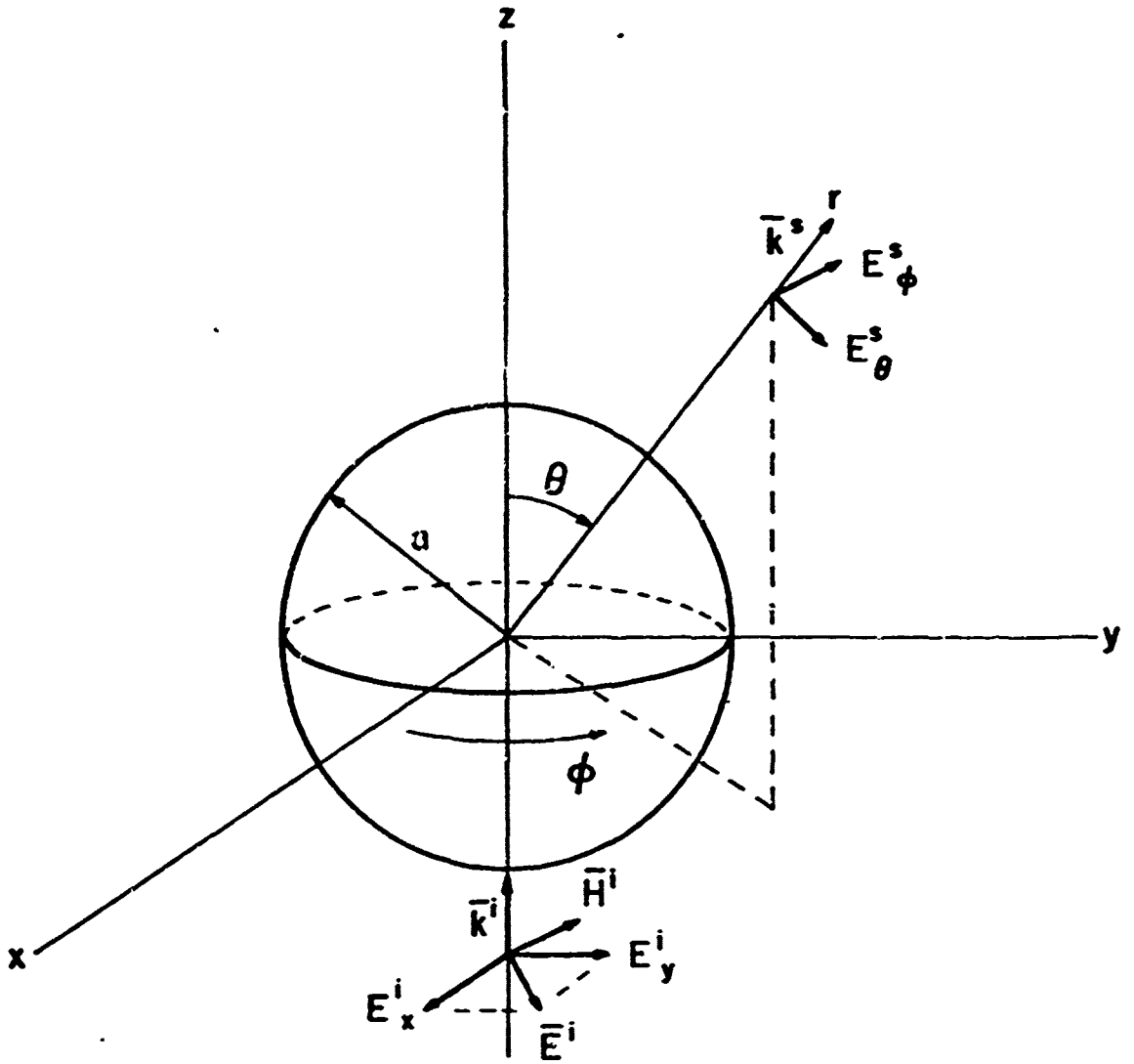

Fig. 1-1. Coordinate system

$$\beta = ka = \frac{2\pi a}{\lambda} \quad , \quad \gamma = mka \tag{1.8}$$

where m is the relative refractive index

$$\psi_n(z) = S_n(z) \tag{1.9}$$

$$\xi_n(z) = \left(\frac{\pi z}{2}\right)^{\frac{1}{2}} H^{(2)}_{n+\frac{1}{2}}(z) \tag{1.10}$$

$$\pi_n(\cos\theta) = \frac{1}{\sin\theta} P^1_n(\cos\theta) \tag{1.11}$$

$$\tau_n(\cos\theta) = \frac{d}{d\theta} P^1_n(\cos\theta) \tag{1.12}$$

Equations (1.9) and (1.10) are the Riccati-Bessel functions and $P^1_n(\cos\theta)$ is an associated Legendre polynomial in equations (1.11) and (1.12).

Clearly the computation of $S_1(\theta)$ and $S_2(\theta)$ presents a formidable calculation. Fortunately there exist tables of computed values for these quantities. If only the intensity of the field is of interest then $|S_1(\theta)|^2$ and $|S_2(\theta)|^2$ will suffice.

If the incident field is linearly polarized then the scattered intensity produced by a beam polarized perpendicular to the observation plane is

$$I_\perp = \frac{\lambda^2}{4\pi^2 r^2} |S_1(\theta)|^2 \tag{1.13}$$

and the scattered intensity produced by a beam polarized parallel to the observation plane is

$$I_\parallel = \frac{\lambda^2}{4\pi^2 r^2} |S_2(\theta)|^2 \tag{1.14}$$

The computation problem then reduces to evaluating the parameters β and m where

$$\beta = \frac{2\pi a}{\lambda} = \frac{\text{Particle Diameter}}{\text{Wavelength in Medium}} \pi \tag{1.15}$$

$$m = \frac{m_1}{m_2} = \frac{\text{Refractive index of scatterer}}{\text{Refractive index of medium}} \tag{1.16}$$

One then finds the tabulated values $|S_1(\theta)|^2$ and $|S_2(\theta)|^2$ corresponding to the given values of β and m and computes the intensity of the scattered field from a single sphere.

Now assume an ensemble of N identical, randomly distributed spheres. Under this assumption the scattered fields are incoherent at any arbitrary observation point. Thus the intensities may be added by superposition and the intensity from the ensemble of N scatterers is just the single sphere intensity multiplied by N.

B. Scattering function for a single, lossless dielectric sphere.

Polystyrene is essentially lossless at optical frequencies so that the refractive index $m_1 = 1.5905$ [5]. The refractive index m_2 of deionized water is $m_2 = 1.332$. Therefore, the relative refractive index, m of the latex particles suspended in water is

$$m = \frac{m_1}{m_2} = 1.194 \tag{1.17}$$

The parameter

$$\beta = \frac{2\pi a}{\lambda} = 3.181 \tag{1.18}$$

where a is the particle radius and λ is the optical wavelength in the medium having refractive index, m_2. If we take

$$\beta = 3.2 \doteq 3.181$$
$$m = 1.2 \doteq 1.194 \tag{1.19}$$

we may use the computed values for $|S_1(\theta)|^2$ and $|S_2(\theta)|^2$ for scattering angles between 0° and 180° in 5° steps [6]. These values are given in Appendix A.

In this experiment the incident beam is linearly polarized in the y direction. The observation plane is the x - z plane, therefore, the incident beam is polarized perpendicular to the observation plane.

A polar plot of I(θ) (Fig. 1-2) illustrates the highly forward character of the scattered intensity.

If a smooth curve is used to connect the discrete points, an analytic function can be constructed which approximates the exact Mie series solution. The approximate function, F(θ) can be used to investigate multiple scattering analytically.

A rectangular plot of I(θ) (Fig. 1-3) suggests a Gaussian function might give close agreement at each discrete point. Let

$$F(\theta) = \exp(-\alpha\theta^2) \quad , -\pi \leq \theta \leq \pi \tag{1.20}$$

Setting F(θ) = I(θ) at the half amplitude point ($\theta = \pm 31°$) requires

$$\exp[-\alpha(.541)^2] = .5 \quad , \quad \alpha = 2.368 \tag{1.21}$$

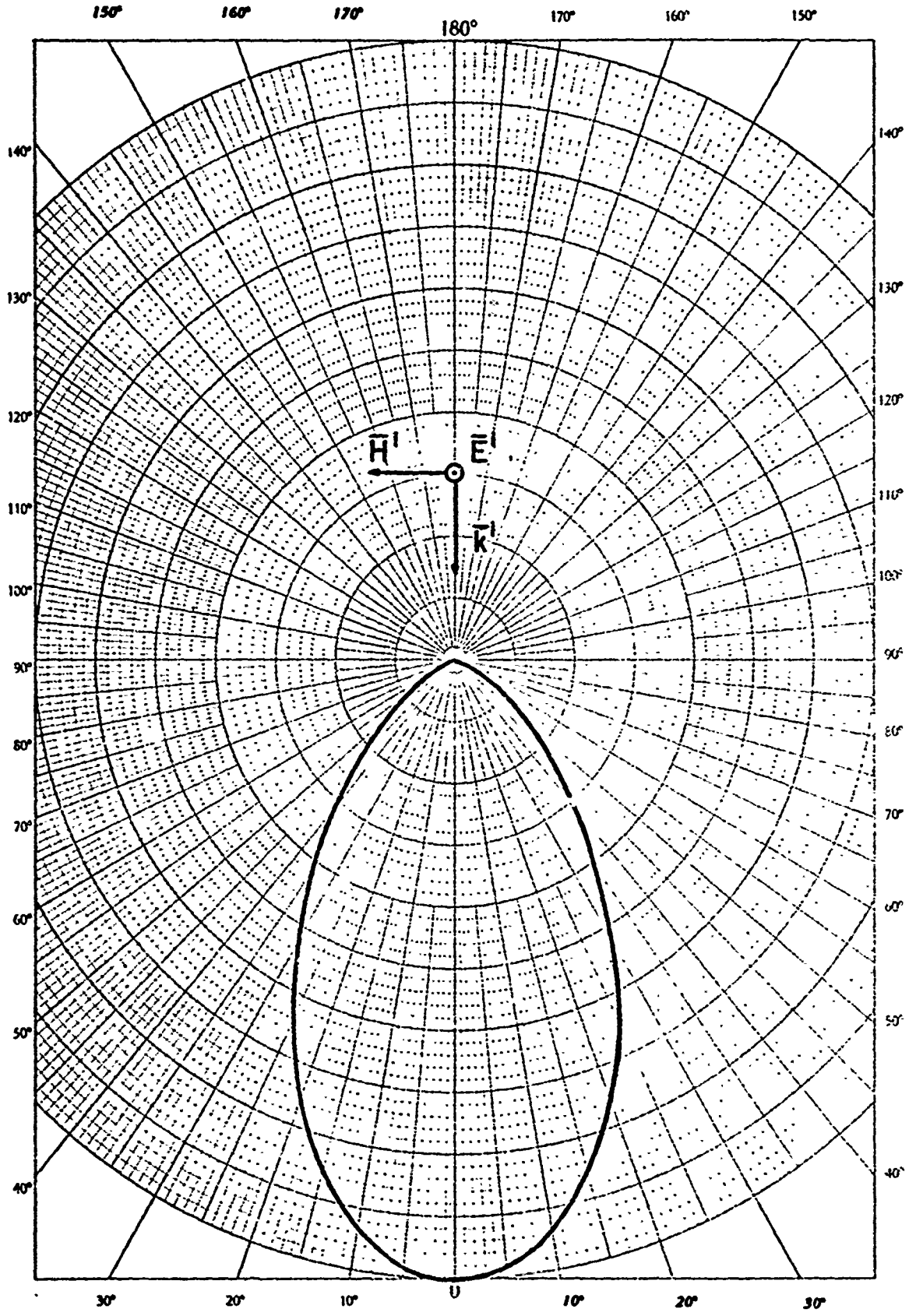

Fig. 1-2. Polar plot of I(θ).

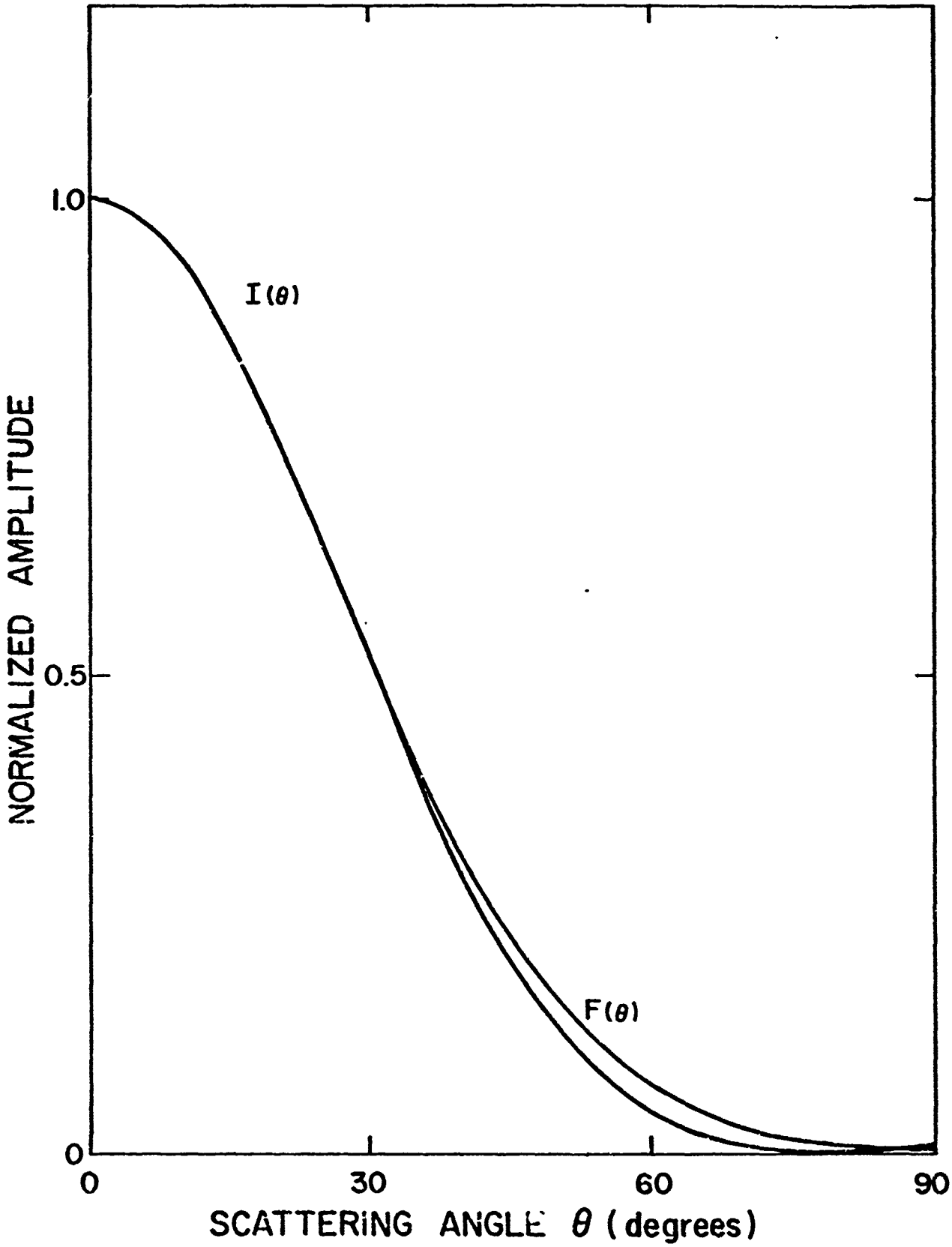

Fig. 1-3. Comparison of I(θ) and F(6).

$$\therefore F(\theta) = \exp(-2.368\,\theta^2)\ ,\ -\pi \leq \theta \leq \pi \tag{1.22}$$

Plotting $F(\theta)$ and $I(\theta)$ on a common scale (Fig. 1-3) it can be seen that these functions are nearly coincident for $|\theta| \leq \pi/6$. Although $F(\theta)$ and $I(\theta)$ differ in the range $\pi/6 < |\theta| \leq \pi$, the error is negligible with respect to multiple scattering calculations.

The probability density function that scattering occurs in a given direction θ, $P(\theta)$ differs from $F(\theta)$ by a normalization constant, A. Requiring

$$\int_{-\pi}^{\pi} P(\theta)\ d\theta = 1 \tag{1.23}$$

or

$$A\int_{-\pi}^{\pi} F(\theta)\ d\theta = 1 \tag{1.24}$$

From symmetry of $F(\theta)$

$$A\int_{-\pi}^{\pi} F(\theta)\ d\theta = 2A\int_{0}^{\pi} F(\theta)\ d\theta \tag{1.25}$$

We note that

$$\int_{\pi}^{\infty} F(\theta)\ d\theta = 0 \tag{1.26}$$

$$\therefore \int_0^{\pi} F(\theta)\, d\theta = \int_0^{\infty} F(\theta)\, d\theta = \frac{1}{2A} \tag{1.27}$$

$$\int_0^{\infty} \exp(-2.368\ \theta^2) d\theta = \frac{1}{2} \left(\frac{\pi}{2.368}\right)^{\frac{1}{2}} = \frac{1}{2A} \tag{1.28}$$

$$\therefore A = \left(\frac{2.368}{\pi}\right)^{\frac{1}{2}} \quad , \quad P(\theta) = \left(\frac{2.368}{\pi}\right)^{\frac{1}{2}} e^{-2.368\theta^2} \tag{1.29}$$

A useful quantity which can be calculated now is the average cosine of the scattering angle θ, $\langle \cos\theta \rangle$

$$\langle \cos\theta \rangle = \int_{-\pi}^{\pi} \cos\theta\ P(\theta)\, d\theta \doteq .90 \tag{1.30}$$

As expected, $\langle \cos\theta \rangle$ indicates a strong forward characteristic.

C. Multiple versus single scattering

1. Analysis of single scattering.

Consider the detector geometry (Fig. 1-4). The following definitions are useful:

ϕ - angular displacement of detector

2θ - detector field-of-view (FOV)

z_o - distance from incident beam entry point ($z = 0$) and detector photocathode

$z(\theta,\phi)$ - intersection of incident beam with limit of detector FOV

The following relations obtain from Fig. 1-5a:

$$a = z_o \sin\theta \tag{1.31}$$

$$\psi = \frac{\pi}{2} - \theta - \phi \tag{1.32}$$

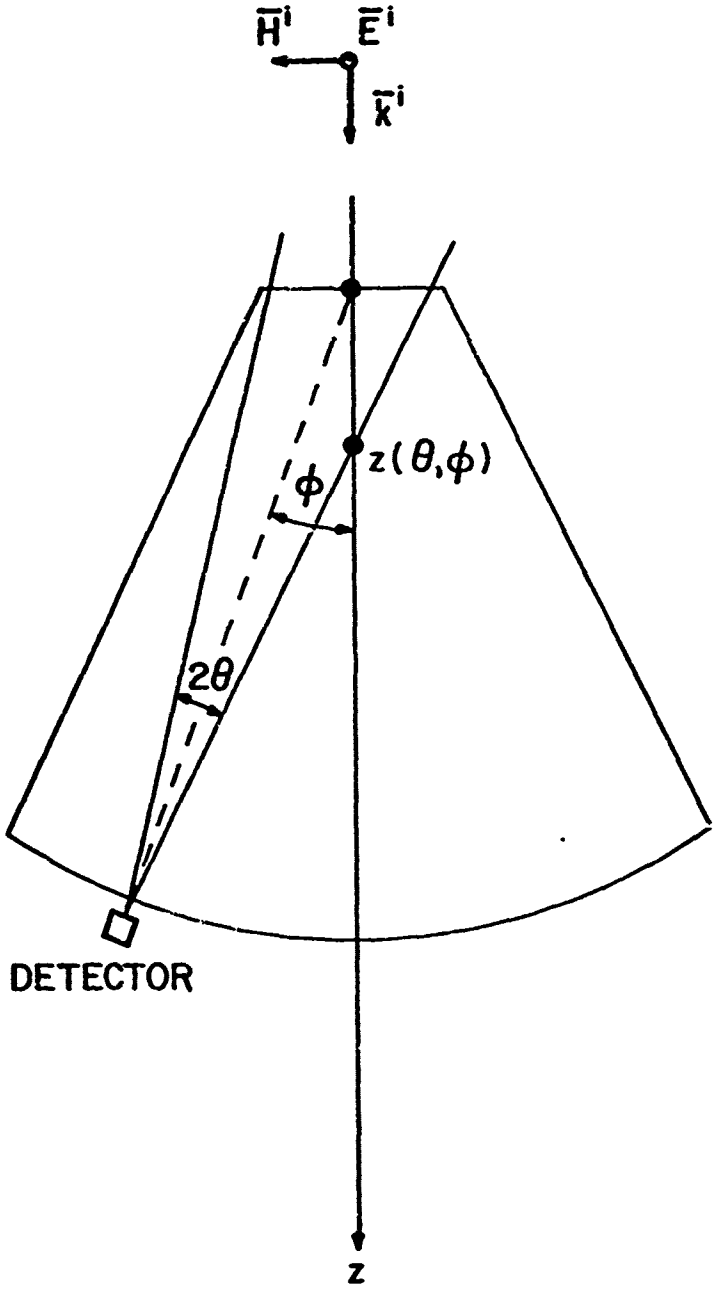

Fig. 1-4. Detector geometry.

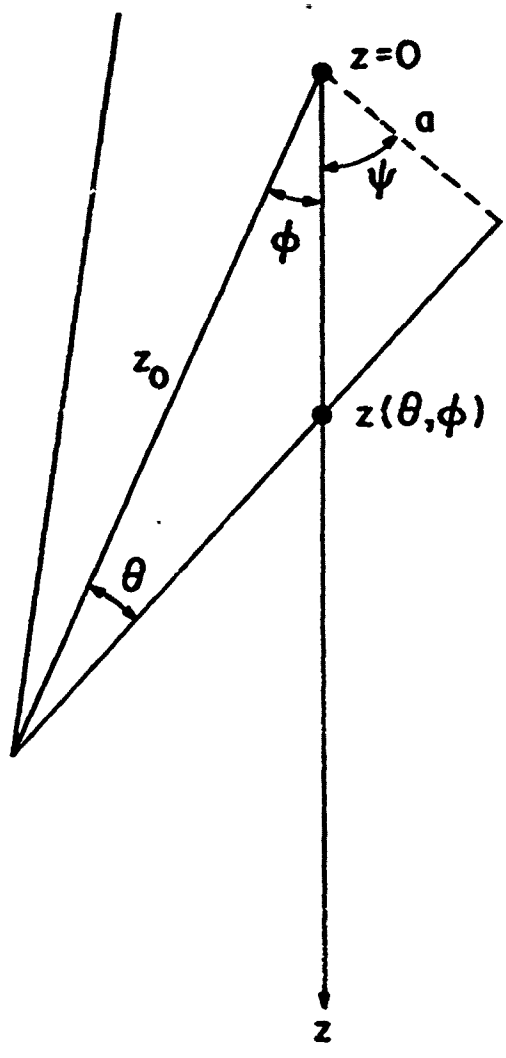

Fig. 1-5a. Single scatter analysis [derivation of $\xi(\theta,\phi)$].

$$z(\theta,\phi) = \frac{a}{\cos \psi} = \frac{z_o \sin \theta}{\cos[\frac{\pi}{2} - (\theta + \phi)]} \tag{1.33}$$

$$z(\theta,\phi) = \frac{z_o \sin \theta}{\sin \theta \cos \phi + \sin \phi \cos \theta} = z_o \quad \xi(\theta,\phi) \tag{1.34}$$

where

$$\xi(\theta,\phi) = \frac{\sin \theta}{\sin \theta \cos \phi + \sin \phi \cos \theta} \tag{1.35}$$

For $0 \leq \phi \leq 12°$ the values of $\xi(\theta,\phi)$ and $z(\theta,\phi)$ (given that $z_o = 31.75$ cm, $\theta = 11°$) are:

ϕ (deg)	$\xi(\theta,\phi)$	$z(\theta,\phi)$ (cm)
0	1	31.75
1	.918	29.15
2	.848	26.92
3	.789	25.05
4	.737	23.40
5	.692	21.97
6	.653	20.73
7	.617	19.59
8	.586	18.61
9	.558	17.72
10	.532	16.89
11	.509	16.16
12	.488	15.49

Table 1-1 $\xi(\theta,\phi)$ and $z(\theta,\phi)$

Assume a single scattering event occurs as a given photon propagates through the chamber. Let $z(\theta,\phi)$ be the coordinate where this event occurs. The following relations obtain from Fig. 1-5b:

$$s = z(\theta,\phi) \cos \phi \tag{1.36}$$

$$z' = \frac{z_o - s}{\cos \theta} = \frac{z_o - z(\theta,\phi) \cos \phi}{\cos \theta} \tag{1.37}$$

$$z' = \frac{z_o - z_o \xi(\theta,\phi) \cos \theta}{\cos \theta} \tag{1.38}$$

$$z' = \frac{z_o (1 - \xi(\theta,\phi) \cos \phi)}{\cos \theta} \tag{1.39}$$

Note that the change in path length, ΔL

$$\Delta L = [z(\theta,\phi) + z'] - z_o \tag{1.40}$$

Equation (1.40) gives the limiting value of ΔL for single scattering. The time delay, Δt for a photon traveling the differential path length ΔL is given by

$$\Delta t = \frac{\Delta L}{c} \tag{1.41}$$

where c is the propagation velocity of light in the medium having refractive index m_2.

Consider the special case of propagating optical pulses which are periodic with period, T. Suppose signals are derived from both the un-

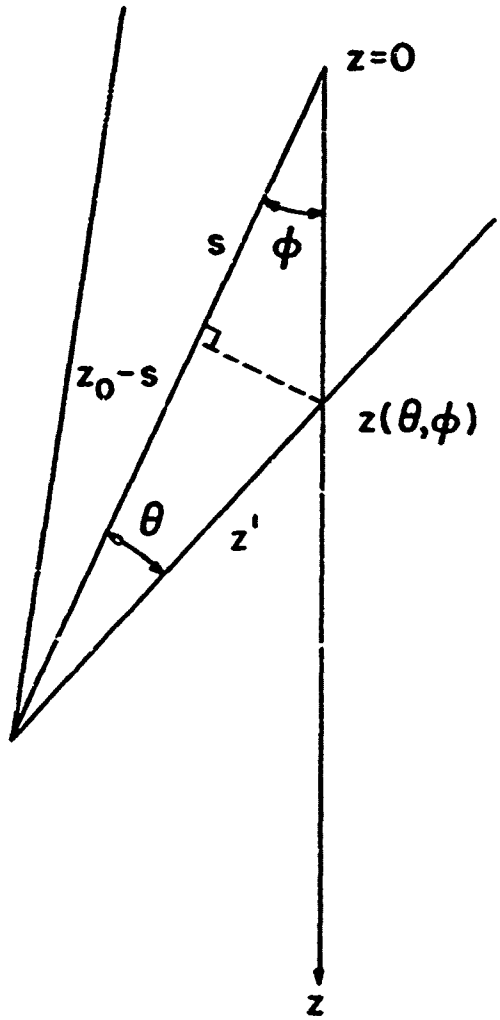

Fig. 1-5b. Single scatter analysis (full field of view).

scattered main beam and the scattered intensity at some arbitrary position, ϕ. Of course, these signals retain the periodic nature of the optical pulses and a phase difference $\Delta\alpha$ exists between the two periodic signals. We note that

$$\frac{\Delta\alpha}{2\pi} = \frac{\Delta t}{T} \tag{1.42}$$

where T = 13.14 nanoseconds. Solving Equations (1.39) through (1.42) we obtain the following values:

ϕ(deg)	$z(\theta,\phi)$(cm)	z'(cm)	ΔL(cm)	Δt(psec)	$\Delta\alpha$(deg)
0	31.75	0	0	0	0
1	29.16	2.643	.053	2.35	.064
2	26.92	4.937	.107	4.75	.13
3	25.06	6.850	.160	7.10	.20
4	23.40	8.564	.214	9.50	.26
5	21.98	10.038	.268	11.88	.33
6	20.74	11.332	.322	14.27	.39
7	19.60	12.526	.376	16.68	.46
8	18.62	13.560	.430	19.08	.52
9	17.72	14.515	.485	21.49	.59
10	16.90	15.389	.539	23.92	.66
11	16.16	16.184	.594	26.35	.72
12	15.50	16.899	.649	28.78	.79

Table 1-2

Assume now that the single scattering event occurs at $\frac{z(\theta,\phi)}{2}$. This is the coordinate of the intersection of the incident beam with the restricted FOV, θ.

The following relations obtain from Fig. 1-5c:

$$s = \frac{z(\theta,\phi)}{2} \cos \phi \tag{1.43}$$

$$z' = \frac{z_o - s}{\cos \frac{\theta}{2}} = \frac{z_o - \frac{z(\theta,\phi)}{2} \cos \phi}{\cos \frac{\theta}{2}} \tag{1.44}$$

$$z' = \frac{z_o(1 - \frac{\xi(\theta,\phi) \cos \phi}{2})}{\cos \frac{\theta}{2}} \tag{1.45}$$

$$\Delta L = [\frac{z(\theta,\phi)}{2} + z'] - z_o \tag{1.46}$$

Solving equations (1.45), (1.46), (1.41) and (1.42) (given that $\theta = 11°$, $z_o = 31.75$ cm) we obtain the values shown in Table 1-3. It is clear from the results summarized in Tables 1-2 and 1-3 that a progressive multipath delay results at viewing positions displaced from the main beam. However, even in the limiting case of $\phi = 12°$, Δt is less than 30 picoseconds. If we assume a typical pulse width of 300 picoseconds, this delay is probably negligible. Indeed, if on the average only a single scattering event occurs, then much of the signal energy will be confined to the main beam and those photons which are delayed make a negligible contribution to the total received pulse. Thus multipath time spreading from single scattering is negligible in so far as data rate limitation is concerned.

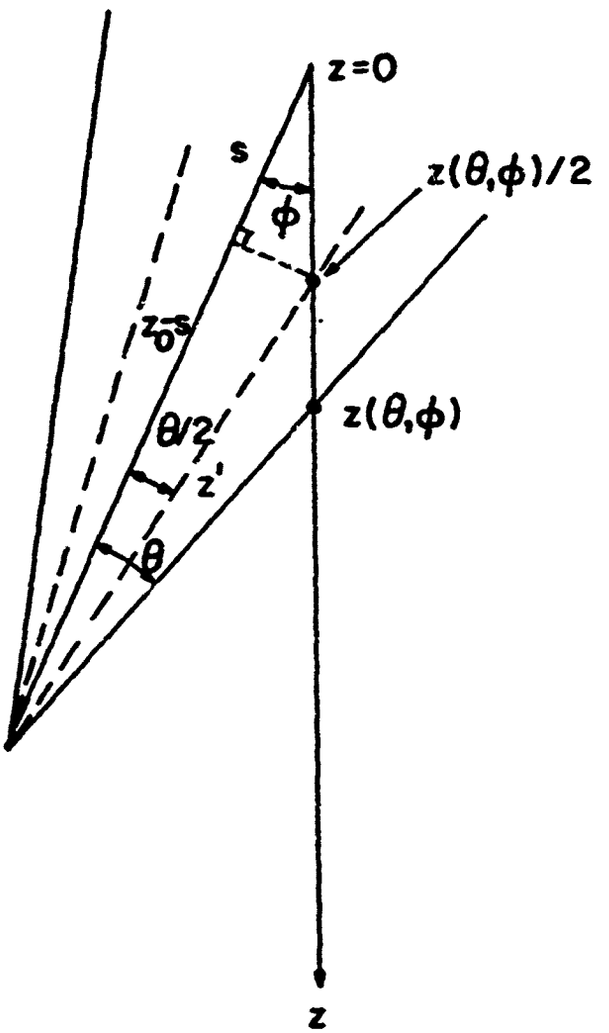

Fig. 1-5c. Single scatter analysis (restricted field of view).

ϕ(deg)	$\frac{z(\theta,\phi)}{2}$(cm)	z'(cm)	ΔL(cm)	Δt(psec)	$\Delta\alpha$(deg)
0	15.89	0	0	0	0
1	14.58	17.252	.082	3.62	.10
2	13.46	18.383	.093	4.12	.11
3	12.53	19.326	.106	4.71	.13
4	11.70	20.171	.121	5.38	.15
5	10.99	20.898	.138	6.12	.17
6	10.37	21.536	.156	6.91	.19
7	9.80	22.125	.175	7.75	.21
8	9.31	22.635	.195	8.64	.24
9	8.86	23.105	.215	9.55	.26
10	8.45	23.537	.237	10.50	.29
11	8.05	23.929	.259	11.47	.31
12	7.75	24.281	.281	12.46	.34

Table 1-3

2. Multiple Scattering

The analysis of single scattering indicates that it does not introduce significant multipath time spreading. Thus multipath scattering events must be considered. It is clear that a simple geometrical analysis analogous to that used for the single scatter case does not exist. The multiple scattering problem is generally analyzed using radiative transfer theory [7] or by performing a Monte Carlo simulation [8].

A typical Monte Carlo photon path simulation is depicted in Fig. 1-6. The incident photon travels a distance d_i to the i-th scatter event. A new propagation direction Φ_i is selected relative to the i-th direction. Note that Φ_i is a function of the scattering angle, θ_i and the polar

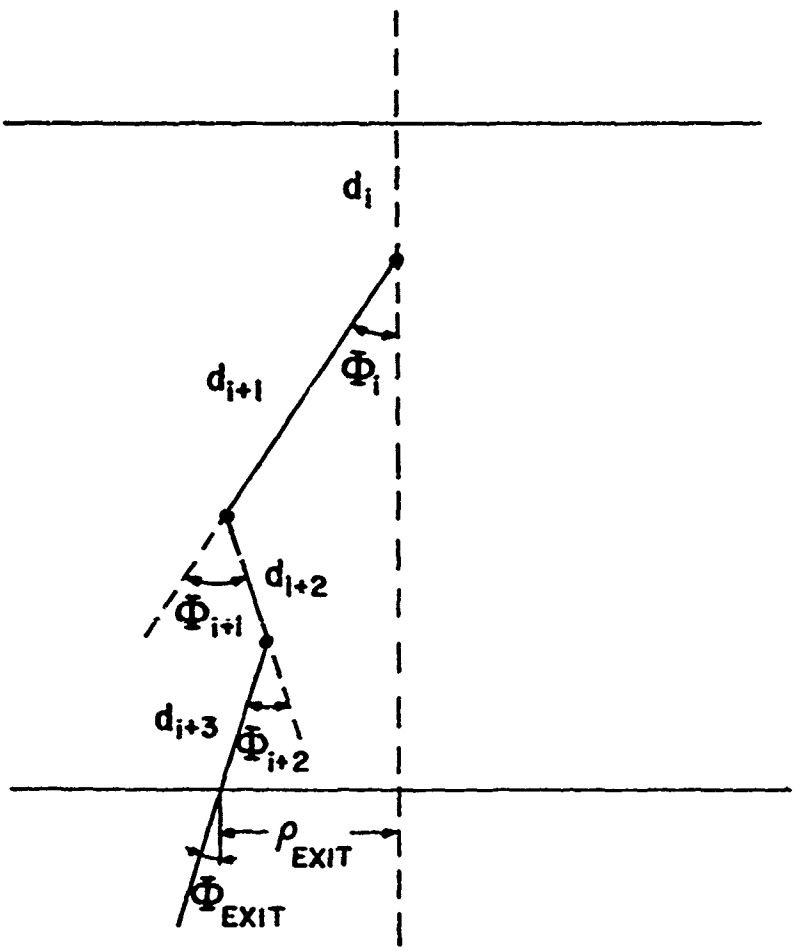

Fig. 1-6. Monte Carlo photon path simulation.

angle, ϕ_i. The process is repeated until the photon exits the simulated medium. The parameter d_i is a random variable with probability density $P(d_i)$ related to the mean free path between scatters. θ_i is a random variable with probability density $P(\theta_i)$ determined by scattering function. ϕ_i is a uniformly distributed random variable. Typically the total distance traveled, exit angle and radius of the exit point from the main beam are recorded for each transmitted photon. After a large number of these events have been collected, the data is reduced to obtain a representative statistical sample of all paths. An analysis of multipath time spreading may then be obtained from the differential path lengths.

SECTION 2

EXPERIMENT

A. Equipment and configuration description

The optical source is a Spectra-Physics Model 125 He:Ne laser operating at 6328Å (Fig. 2-1). The mode locked output is a train of 1.5 nanosecond (at half amplitude) pulses with period of 13.14 nanoseconds (76 MHz) and average power of 25 milliwatts. A beam splitter diverts a small amount of the beam to an RCA 931A photomultiplier the output of which produces the reference RF signal.

The main beam passes through a wedge variable attenuator and into the scattering chamber. An RCA 8644 Photomultiplier detects the scattered intensity at any desired viewing position. Aperture stops control the detector field-of-view and a rotatable polarizer selects the desired orientation of polarization of scattered intensity.

Each photomultiplier output is followed by a narrow pass-band filter centered at the fundamental frequency, thus higher order frequency components are rejected.

The filtered outputs are applied to the sampling probes of the Hewlett-Packard 8405A Vector Voltmeter. The RF envelopes are frequency translated to an intermediate frequency (IF) and the IF signals are filtered to obtain inputs for the voltmeter and phasemeter.

The scattering chamber was designed so that the geometric path length between the incident beam entry point and the viewing position at the detector was independent of the angle ϕ, (Fig. 2-2). This was accomplished by making the output window of the chamber the surface of a right circular cylinder whose center is located at the incident beam entry point. The detector is mounted on a swing arm with pivot

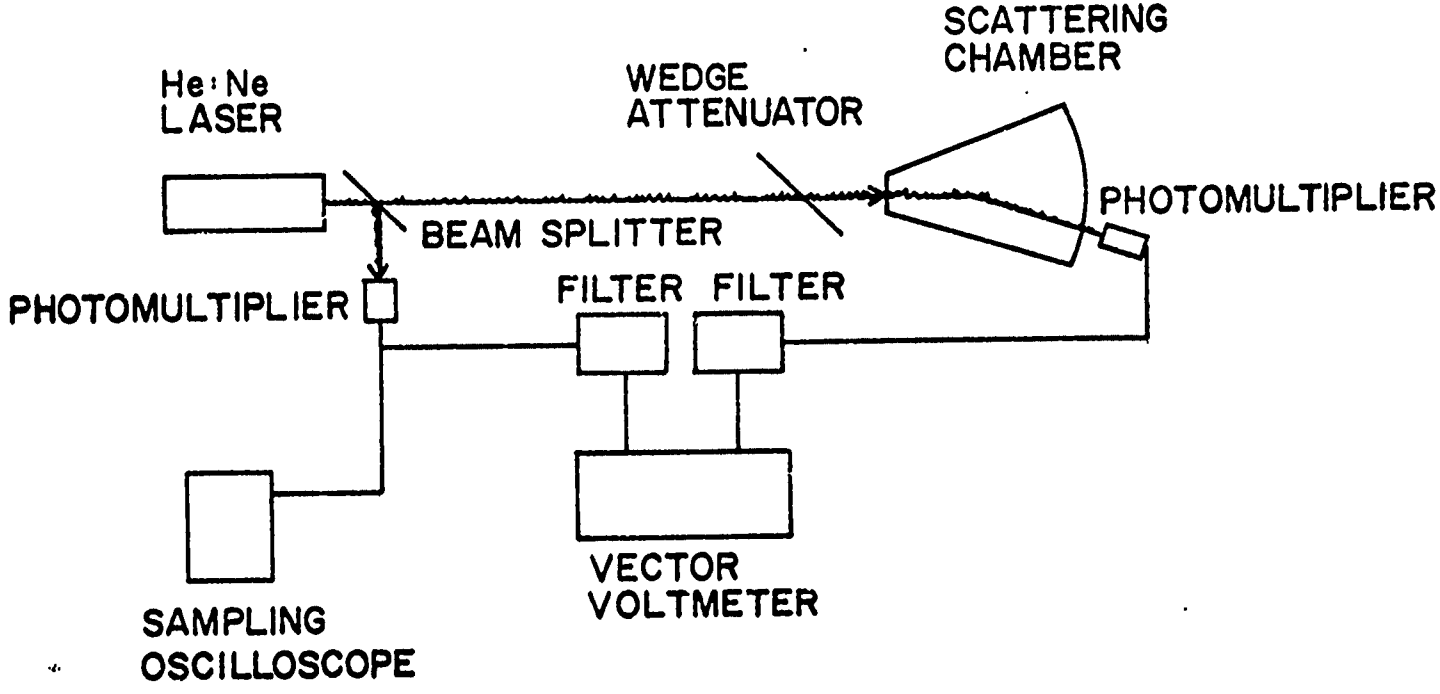

Fig. 2-1. Schematic diagram of experiment components.

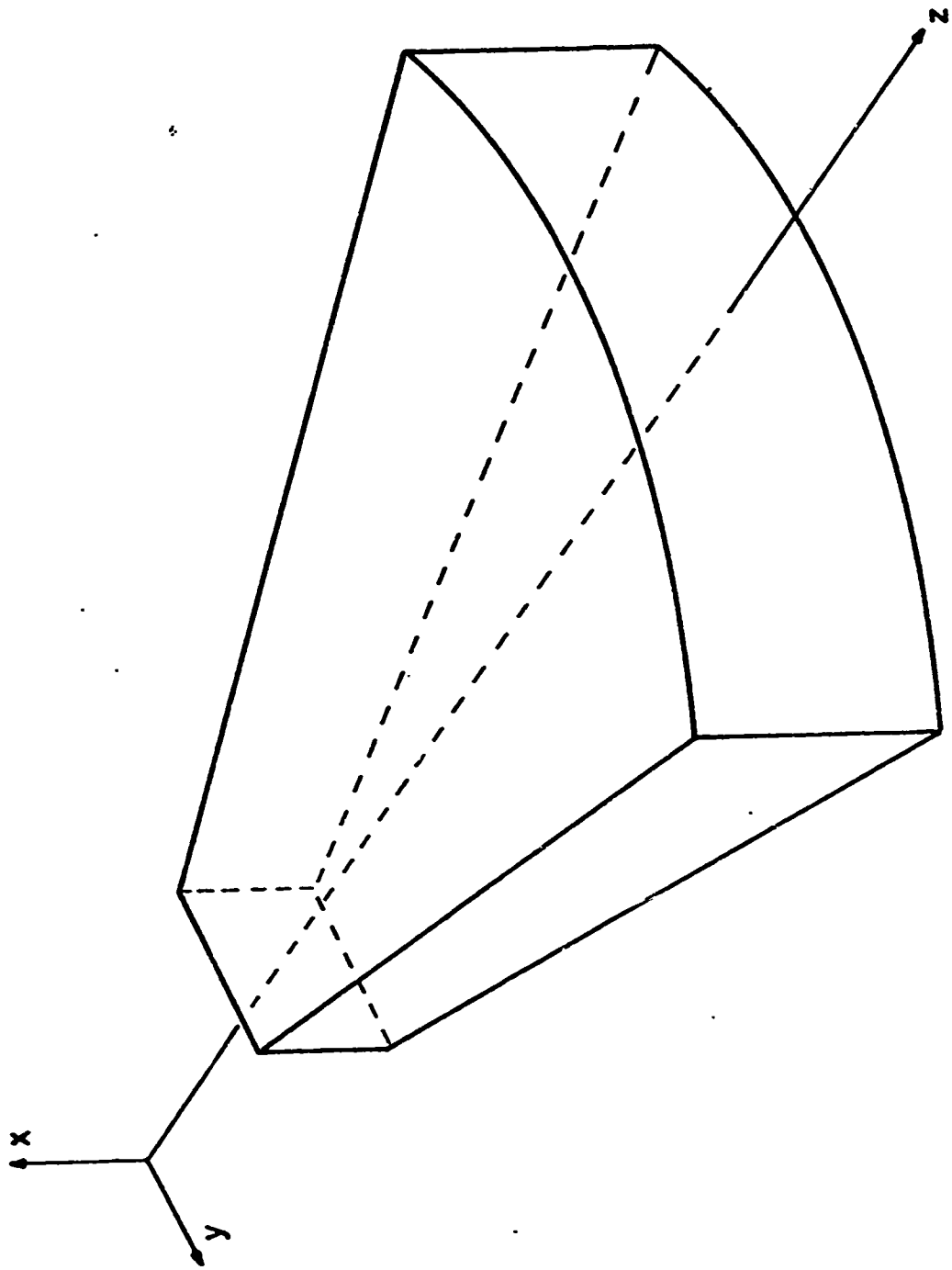

Fig. 2-2. Scattering chamber.

point also located directly above the incident beam entry point.

The semi-infinite extent of the scattering medium (in the directions transverse to the axis of propagation) was simulated by making the transverse dimensions much larger than the diameter of the incident beam and by painting the interior bottom, side and top surfaces with flat black paint to minimize reflections. The entrance and exit windows of the chamber were fabricated from clear plexiglass acrylic sheets. The volume of the chamber is approximately 3 liters.

Consider the result of allowing the detector to scan all angles ϕ such that the received signal is the sum over all ϕ. An effective field-of-view can be defined (Fig. 2-3).

$$FOV_{eff} = 2\theta + 2\phi$$

The effective FOV (given that $\theta = 11°$, $\phi = 12°$) is 46°. Such a FOV is unrealistically large for a real system however it should be noted that this results from the large angles needed to generate measureable multipath delays with laboratory scale media.

Initially a highly dilute mixture of skim milk and distilled water was used as a scattering medium. Casein micelles in skim milk act as highly hydrated spheres of mean radius 800Å. Approximately 95% of these are in the range 400-2200Å, [9]. Thus the larger micelles have strong forward scattering characteristics at 6328Å. Milk has the advantages of being readily available and relatively inexpensive. The disadvantages are short shelf life and the uncertainty as to exact distribution of particle size and number.

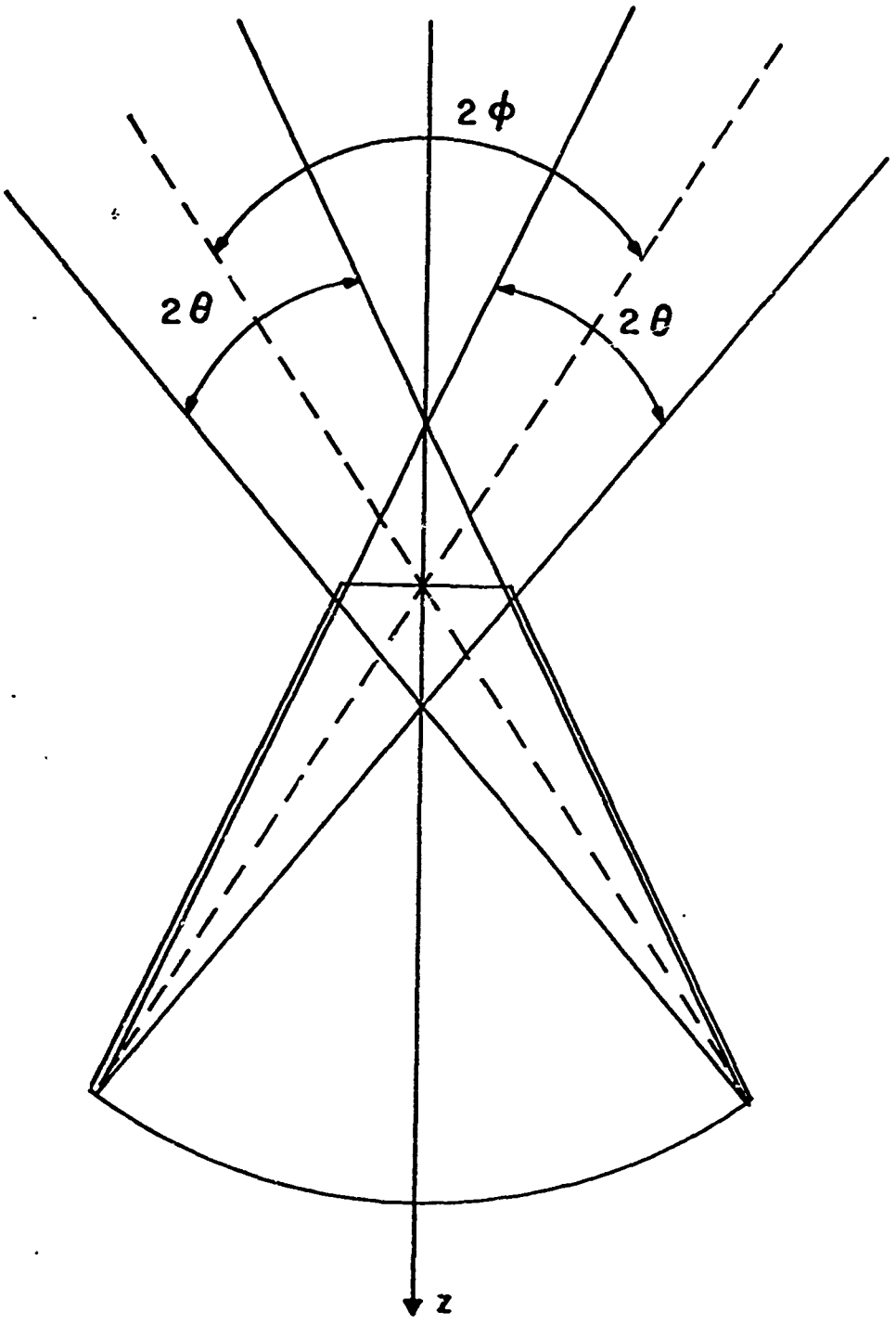

Fig. 2-3. Detector effective field of view.

Experiments were also conducted using monodisperse uniform latex particles manufactured by Dow Diagnostics. The 0.481 micron diameter Polystyrene particles were used to obtain strong forward scattering. These particles are spherical while suspended in deionized water and have extremely uniform radii (standard deviation 18 Å). The concentration (number of particles per milliliter) was calculated from technical data supplied by the manufacturer and verified by measuring the extinction coefficient of a dilute suspension of the particles. (For details refer to Appendix B).

The concentrations used resulted in a scattering medium having an optical thickness in the range of 1-2. (See Appendix C).

B. Measurement procedure

Initial time dispersion measurements were attempted by observing the scattered pulse in real time using the Sylvania 502 crossed field photomultiplier and Tektronix Sampling Oscilloscope. No pulse broadening was evident and it was assumed that the magnitude of the broadening was beyond the resolution capability of this measurement system.

The measurement technique adopted is analogous to that used to measure group delay in electrical transmission lines. The application of this method requires a periodic radio frequency (RF) signal, a condition satisfied by the mode locked He:Ne laser. The incident and scattered intensities are used to derive two RF signals whose relative phase relationships are compared. Time delay is then deduced from the phase measurements.

C. Analysis of measurement errors

The only measurement errors considered are those relating to the relative phase between incident and scattered signal waveforms. These errors may result from

1. Difference in relative signal levels,

2. Systematic variation, or

3. Detector translation

1. Difference in relative signal levels

The primary range of this error occurs when Channel B amplitude varies between 5 mV and 25 mV producing a phase change of about 2.5 degrees. Below 1 mV the phase changes due to changing relative amplitude are negligible.

A wedge attenuator with 10:1 intensity attenuation ratio was used to obtain a calibration curve (phase correction vs Channel B amplitude) and all raw data was adjusted using the appropriate correction prior to analysis.

2. Systematic variation

In general, the phase fluctuated about a mean value during measurement with average variation of ± 0.2 degrees. The phase values recorded were obtained by estimating the mean value during the observation interval usually 5 to 10 seconds. Additionally, a chart recorder was used on selected data runs to illustrate typical variation conditions (Fig. 2-4).

3. Detector translation

Mechanical slack at the swing arm hinge point allows slight translation of the detector. However, the maximum variation is 0.01 mm and the resulting phase error is negligible.

D. Summary of results

1. Effect of experiment parameters on phase shift

a. Detector polarizer

Measurements were made with the polarizer oriented both parallel and

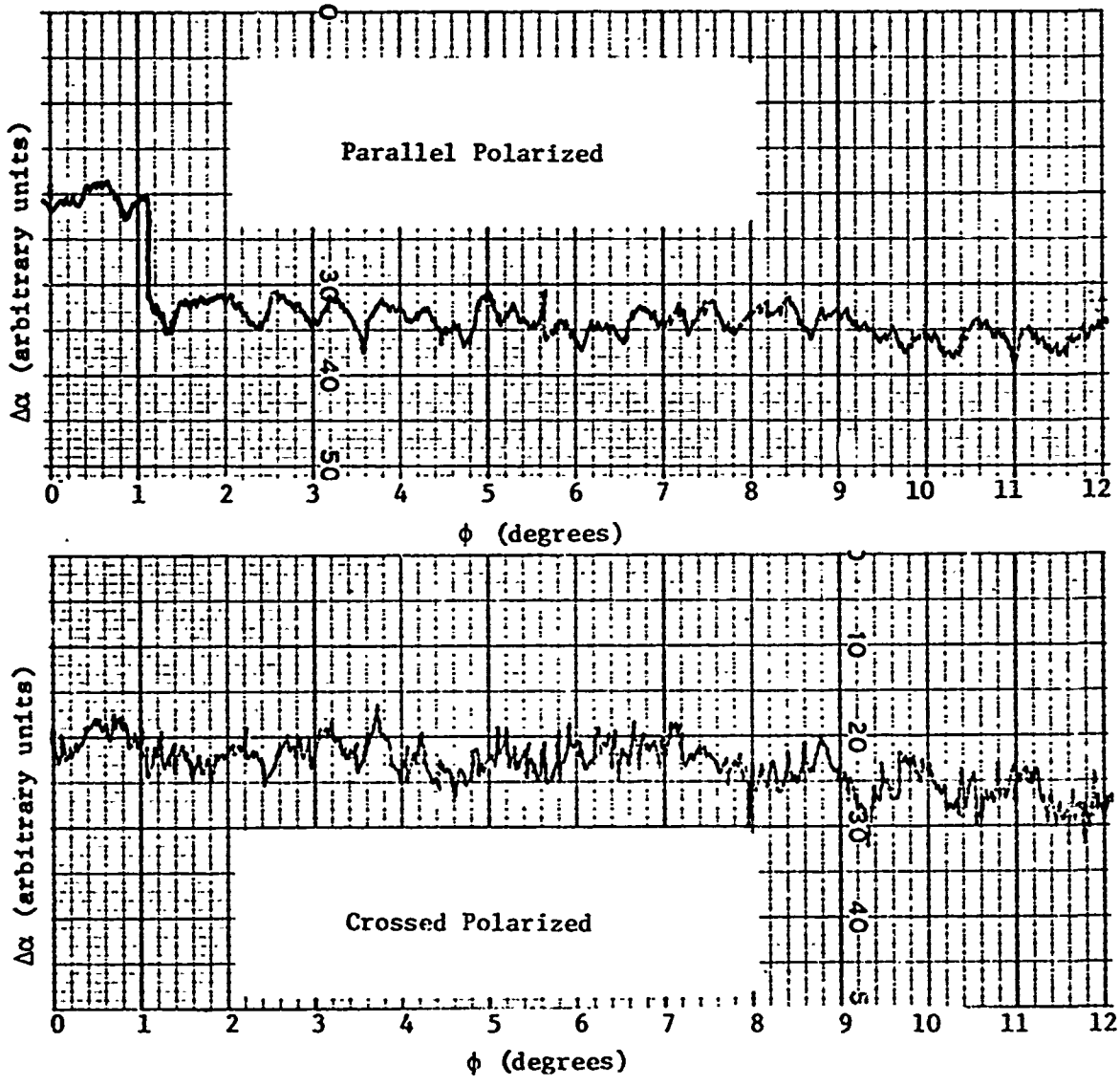

Fig. 2-4. Typical systematic variation of phase angle.

perpendicular to the incident beam polarization. No significant difference in the phase shift was apparent.

b. Aperture

Several apperture sizes were used. The phase shift and aperture size are directly related since the aperture controls the FOV.

c. Scatterer density

Several different concentrations were used, each producing similiar phase shifts. At the highest density the signal level at the vector voltmeter was insuffi ient for reliable and repeatable measurements, thus, the scatterer density wa restricted to a rather narrow range between $10^8 cm^{-3}$ and $4 \times 10^8 cm^{-3}$.

2. Review of results

The results were obtained with detector aperture and FOV as described in Section 1.C. The minimum phase shift measured was 0.7 degrees; the maximum was 1.9 degrees and the mean was 1.25 degrees for 21 trials. At low scatterer densities the intensity of the central beam caused excessive photomultiplier current, therefore, all phase measurements were taken between $\phi = 2°$ and $\phi = 12°$ ($\phi = 2°$ corresponds to a detector position clear of the central beam). A typical plot is shown in Fig. 2-5.

At the maximum scatterer density the effective optical thickness of the medium was slightly less than 2. Thus, it is not surprising that the phase shift is comparable to that expected from single scattering since the expectation of the number of scattering events for a given photon is on the order of 1 or 2.

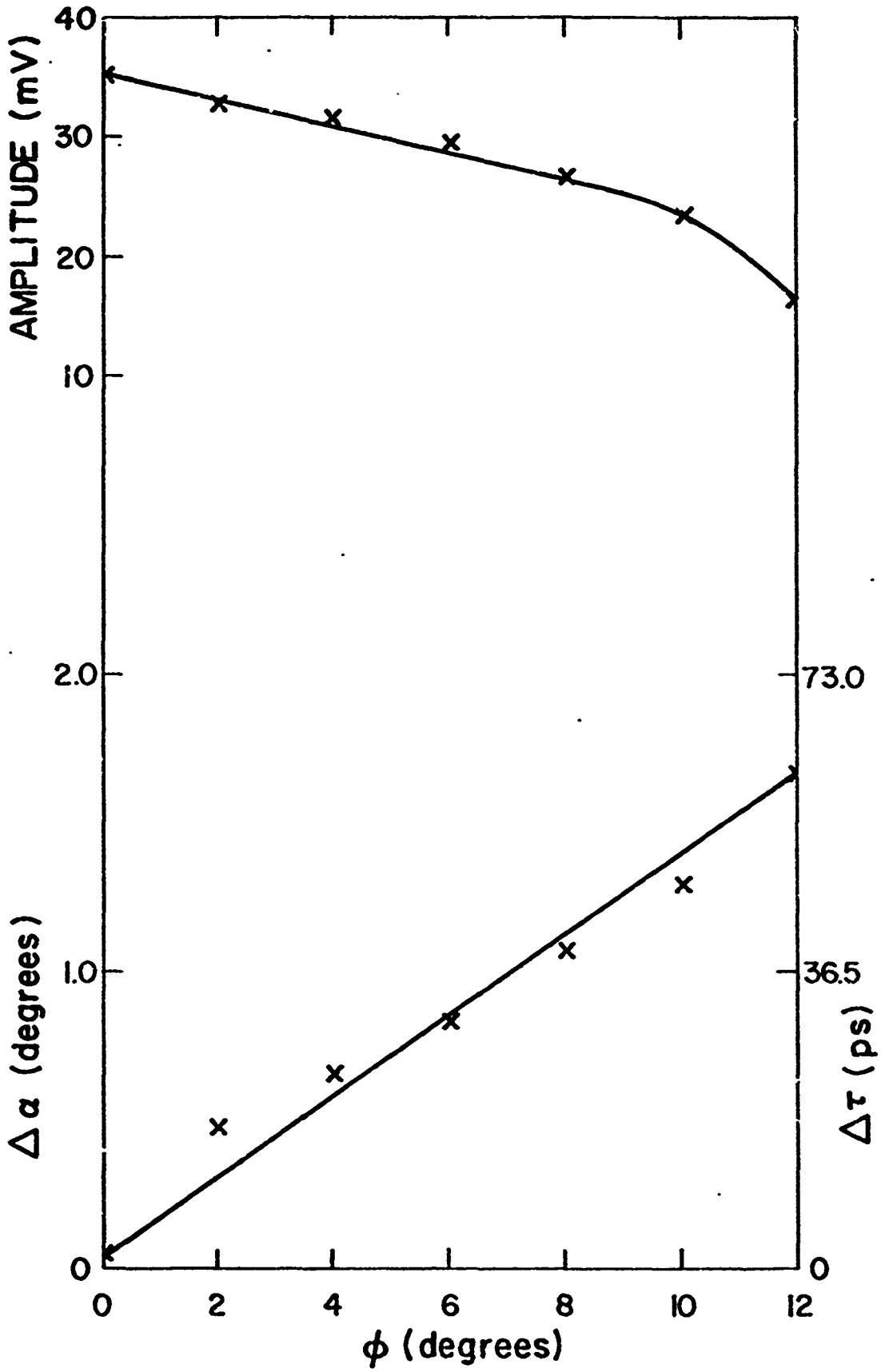

Fig. 2-5. Typical phase variation.

CONCLUSIONS

The time delays measured in this experiment did not produce significant time spreading of the He:Ne mode locked pulse. Neither would they produce significant time spreading of much shorter pulses typical of operational optical communication systems. This is consistent with the fact that single scattering was the dominant mechanism producing the multipath delays. It has been pointed out that the relatively low intensity (25 mW) of the optical source restricted the maximum scattering medium density which could be used while assuring adequate intensity at the detector. This restriction lead to predominantly single scattering.

The measurement of multipath delay by using the comparison of relative phase of the (periodic) incident and scattered pulse envelopes circumvents the detector rise time limitations and could be applied to measurements with much shorter pulses.

Further experimentation is needed using shorter, more intense pulses. One possibility would be a mode locked Argon ion laser. Such a source could provide pulses in the 300 picosecond range and power on the order of watts. The increased intensity is essential to increasing the optical thickness of the medium producing multiple scattering events.

For large optical thickness, Bucher's computer simulations predict multipath delays of nanoseconds. If the main beam has suffered great extinction and the receiver field of view has been increased to collect scattered photons, the delayed photons may produce very significant time spreading of the received pulse. For example, a 300 picosecond pulse system with 300 picosecond guard time has a potential data rate of 1.67 Gigabits/sec. In the event the pulses are spread by multipath processes to 1 nanosecond the data rate is reduced to 770 Megabits/sec.

The effects of multipath pulse spreading on the potential data rate of currently feasible, state of the art optical communications systems are far more profound. Consider a mode locked dye laser capable of generating 1 picosecond pulses; beam superposition techniques can be used to produce a periodic pulsed output with period of several picoseconds (say 10 picoseconds); in a synchronized link, such pulses can be resolved with optoelectronic sampling [10]. Such a system has a potential data rate of 100 Gigabits/sec; however, multipath pulse spreading of 1 nanosecond would reduce it by a factor of 100. Thus it is apparent that multipath pulse spreading produces severe limits for ultra short pulse, high data rate optical communications systems.

LIST OF REFERENCES

1. G.N. Plass and G.W. Kattawar, "Monte Carlo Calculations of Light Scattering from Clouds," App. Opt., vol. 7, pp. 415-419, March 1968.
2. E.A. Bucher, "Computer Simulation of Light Pulse Propagation for Communication Through Thick Clouds," App. Opt., vol. 12, pp. 2391-2400, October 1973.
3. W.G. Blattner, B.C. Thompson, and M.B. Wells, Transport of Laser Radiation in Foggy and Turbulent Atmospheres, Fort Worth: Radiation Research Associates, Inc., 1971.
4. H.C. Van de Hulst, Light Scattering by Small Particles, New York: Wiley, 1957, pp. 114-130.
5. Handbook of Chemistry and Physics, Cleveland: The Chemical Rubber Co., 1969, p. C-769.
6. W.J. Pangonis and W. Heller, Angular Scattering Functions for Spherical Particles, Detroit: Wayne State University Press, 1960, p. 131.
7. S. Chandrasekhar, Radiative Transfer, New York: Dover, 1960.
8. Y.A. Shreider, The Monte Carlo Method; The Method of Statistical Trials, New York: Pergamon, 1966.
9. R.K. Dewan, A. Chudgar, R. Mead, V.A. Bloomfield, and C.V. Morr, "Molecular Weight and Size Distribution of Bovine Milk Casein Micelles," Biochim. Biophys. Acta, vol. 342, pp. 313-321, March 1974.
10. H. Merkelo, J.J. Wiczer, and P.R. Buttinger, "Optoelectronic Sampling--I. Parameters for Picosecond Resolution," to be published.
11. N.C. Wickramasinghe, Light Scattering Functions for Small Particles with Applications in Astronomy, New York: Wiley, 1973, p. 55.

12. E.A. Bucher and R.M. Lerner, "Experiments on Light Pulse Communication and Propagation Through Atmospheric Clouds," App. Opt., vol. 12, p. 2410, October 1973.

APPENDIX A

Let $I_\perp$ be defined as the intensity of the wave scattered by a single sphere from an incident beam of unit intensity with polarization perpendicular to the observation plane.

$$I_\perp = \frac{\lambda^2 \alpha^2}{4\pi^2 r^2} \frac{i_\perp}{\alpha^3} \tag{A.1}$$

where λ is the wavelength in the medium and

$$\alpha^3 \equiv x^3 = \left(\frac{2\pi a}{\lambda}\right)^3 \tag{A.2}$$

as previously defined and $\frac{i_\perp}{\alpha^3}$ is the tabulated value for the far field ($r >> \lambda$) at the angle γ.

Since γ is the angle of observation with respect to the reverse direction of the incident beam, γ is related to θ by

$$\theta = \pi - \gamma \tag{A.3}$$

The following values for $\frac{i_\perp}{\alpha^3}$ as a function of γ assume $\alpha = 3.2$, $m = 1.2$, (Table A-1):

m = 1.20

α = 3.2

γ	$i_\perp/\alpha^3$	$i_\parallel/\alpha^3$	i_T/α^3
0	0.0014914	0.0014914	0.0029828
5	0.0014827	0.0014641	0.0029468
10	0.0014655	0.0013861	0.0028516
15	0.0014650	0.0012687	0.0027337
20	0.0015198	0.0011277	0.0026475
25	0.0016770	0.00097987	0.0026569
30	0.0019853	0.00083922	0.0028246
35	0.0024863	0.00071441	0.0032007
40	0.0032041	0.00060789	0.0038119
45	0.0041388	0.00051714	0.0046559
50	0.0052524	0.00043922	0.0056916
55	0.0064624	0.00037582	0.0068382
60	0.0076453	0.00033728	0.0079826
65	0.0086325	0.00034508	0.0089775
70	0.0092297	0.00042743	0.0096571
75	0.0092484	0.00061006	0.0098584
80	0.0085504	0.00090357	0.0094540
85	0.0071135	0.0012955	0.0084090
90	0.0050997	0.0017559	0.0068556
95	0.0029466	0.0022751	0.0052217
100	0.0014406	0.0029429	0.0043836
105	0.0017651	0.0040731	0.0058382
110	0.0055021	0.0063617	0.011864
115	0.014566	0.011042	0.025608
120	0.031043	0.019976	0.051019
125	0.056955	0.035614	0.092569
130	0.093922	0.060756	0.15468
135	0.14281	0.098078	0.24089
140	0.20339	0.14949	0.35288
145	0.27406	0.21539	0.48944
150	0.35173	0.29398	0.64570
155	0.43195	0.38097	0.81292
160	0.50925	0.46973	0.97899
165	0.57767	0.55193	1.1296
170	0.63145	0.61873	1.2502
175	0.66585	0.66248	1.3283
180	0.67769	0.67769	1.3554

Table A-1

APPENDIX B

Determination of N_o

The number of particles per unit volume, N was determined directly by calculation from specifications provided by the manufacturer and indirectly by measurement of the extinciton coefficient. The values obtained in either case agree closely.

Calculation of N

The weight of a single latex sphere, $W = \delta V$ where δ is the density (of polystyrene = 1.05 g/ml) and V is the volume of the sphere. Since $V = \frac{4}{3}\pi(\frac{D}{2})^3$ where D is the diameter = 0.481 μm, then $W = (1.05\ g/ml)\frac{4}{3}\pi \times (2.405 \times 10^{-5}\ cm)^3 = 6.12 \times 10^{-14}$ g. Assume a 1 ml sample of the latex particles in aqueous suspension weighs 1 g. The manufacturer asserts that the sample contains 10% solids by weight. Then the number of particles in a 1 ml sample, N is the total weight of particles divided by the weight of one particle.

$$N = \frac{(1\ g)(.1)}{6.12 \times 10^{-14}\ g} = 1.63 \times 10^{12} \qquad (B.1)$$

Measurement of N

The extinction coefficient, ζ was determined by measuring the transmitted intensity of the He:Ne laser main beam after propagating through a cell containing a highly dilute suspension of the latex particles in deionized water. Using the relation $I_t = I_i \exp(-\zeta L)$, $\zeta = N\pi a^2 Q_{ext}$ where

I_t = transmitted intensity

I_i = incident intensity

L = cell length

N = number of particles

a = radius of particle

Q_{ext} = extinction efficiency = 0.7492
(given by Wickramasinghe [11])

Solving for N we find

$$N = 1.94 \times 10^{12} \tag{B.2}$$

Calculation of N_o

The concentration of scatterers in the chamber per ml of latex particles sample, N_o is equal to $\frac{N}{V}$ where V is the chamber volume = 3000 ml. Using the measured value for N

$$N_o = \frac{1.94 \times 10^{12}}{3 \times 10^{3}\text{ml}} = 6.46 \times 10^{8}\text{cm}^{-3} \tag{B.3}$$

A plot of N_o versus volume of latex particles is given in Fig. B-1.

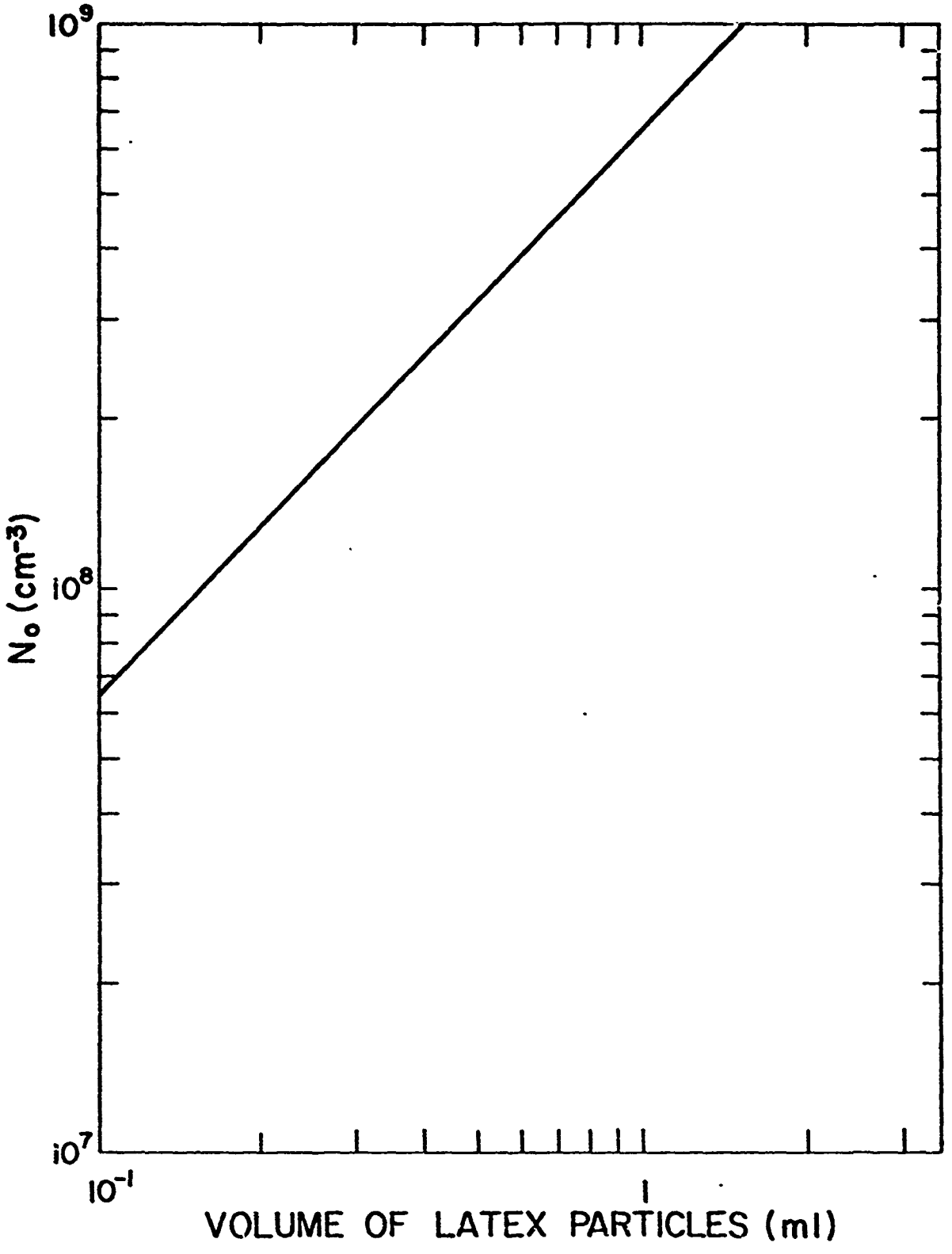

Fig. B-1. Concentration N_o versus volume of latex particles.

APPENDIX C

Calculation of Optical Thickness

The optical thickness, τ is defined as

$$\tau = T/D \tag{C.1}$$

where T is the physical thickness of the medium and D is the mean-free path between scatters. Equation (C.1) is valid for isotropic scatter; for the case of nonisotropic scatter the mean-free path may be replaced by the diffusion distance D_d [12]

$$D_d = \frac{D}{1 - \langle \cos \theta \rangle} \tag{C.2}$$

where $\langle \cos \theta \rangle$ is the average cosine of the scattering angle relative to the incident direction.

In a homogeneous body of scatterers, D is the inverse of the extinction coefficient, ζ. If the scatterers' radii are uniform

$$D = \frac{1}{\zeta} = \frac{1}{Q_{ext} N_o \pi a^2} \tag{C.3}$$

where Q_{ext} is the extinction efficiency factor, N_o is the number of scatterers per unit volume, and a is the scatterer's radius. Substituting (C.3) into (C.2) we obtain:

$$D_d = \frac{1}{Q_{ext} \pi a^2 (1 - \langle \cos \theta \rangle)} \cdot \frac{1}{N_o} \tag{C.4}$$

From (C.1) and (C.2) we obtain an effective optical thickness

$$\tau_d = \frac{T}{D_d} = T\, Q_{ext} \pi a^2 (1 - \langle \cos\theta \rangle) \cdot N_o \qquad \text{(C.5)}$$

Solving (C.4) and (C.5) for D_d and τ_d (given that T = 25.4 cm, $\langle \cos\theta \rangle$ = 0.9, Q_{ext} = 0.7492 [10], and a = 0.481 μm) we find

$$D_d = 7.345 \times 10^9 \text{ cm}^{-2} \cdot \frac{1}{N_o} \qquad \text{(C.6)}$$

$$\tau_d = 3.458 \times 10^{-9} \text{ cm}^3 \cdot N_o \qquad \text{(C.7)}$$

Plots of D_d and τ_d versus N are given in Fig. C-1.

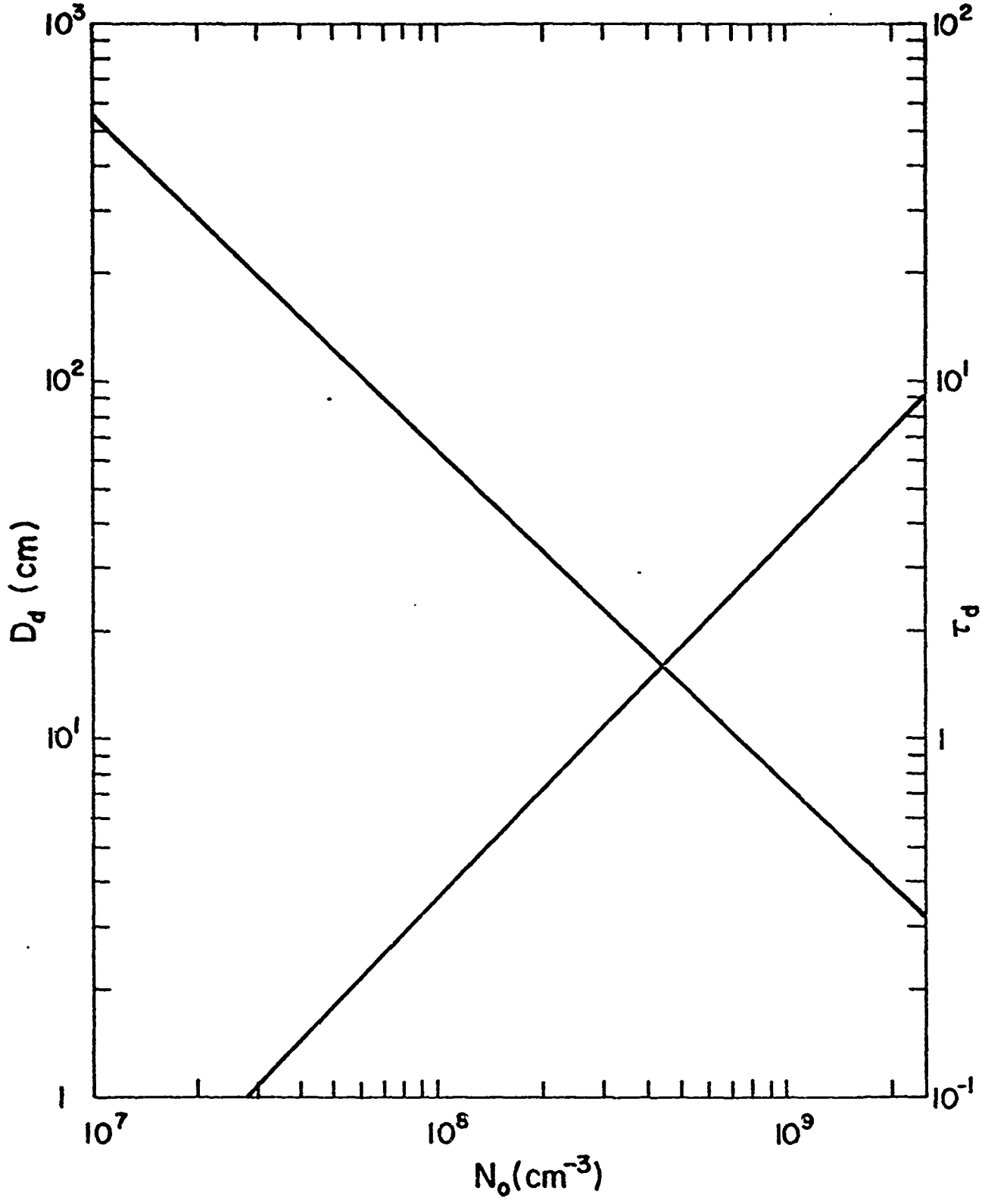

Fig. C-1. Diffusion distance D_d and optical thickness τ_d versus concentration N_o.